




RESEARCH ARTICLE OPEN ACCESS

Nanostructured Anodes for Solid Oxide Fuel Cells Obtained by Screen-Printing and Infiltration

 Martin Michael Juckel¹  | Yanting Liu²  | André Weber² | Olivier Guillon^{1,3} | Norbert H. Menzler¹ 
¹Institute of Energy Materials and Devices, Forschungszentrum Jülich GmbH, Materials Synthesis and Processing (IMD-2), Jülich, Germany | ²Karlsruhe Institute for Technology, Institute For Applied Materials—Electrochemical Technologies (IAM-ET), Karlsruhe, Germany | ³JARA-ENERGY, Jülich, Germany

Correspondence: Norbert H. Menzler (n.h.menzler@fz-juelich.de)

Received: 20 March 2025 | **Revised:** 23 July 2025 | **Accepted:** 18 August 2025

Funding: The project “WirLebenSOFC” was funded by the German Federal Ministry for Economic Affairs and Climate Protection (BMWK), which is gratefully acknowledged (Contract No. 03SF0622B).

Keywords: electrochemical performance | infiltration | nanoparticles | NiO:GDC | stability

ABSTRACT

Nanomaterials were used for the investigation of electrochemical performance tests of solid oxide fuel cells. Two different approaches were chosen to produce symmetrical nanoparticle (NP)-based cells: screen printing and infiltration. Screen printing, as a state-of-the-art manufacturing process, leads to unstable NiO/gadolinium-doped ceria (GDC) conductive layers, which either show delamination or flaking after sintering or electrochemical testing. The infiltration of an NiO scaffold with GDC NPs and the infiltration of a GDC scaffold with NiO NPs, on the other hand, were used as a solution for these problems, and stable symmetrical cells with particle sizes down to 10 nm were produced. All stable infiltrated cells were microstructurally and electrochemically characterized and showed an improved electrochemical performance.

1 | Introduction

Although the principles of solid oxide fuel cells (SOFCs) were already discovered in 1839 by the physicist William Robert Grove, it took far more than 100 years until the first applications could be implemented [1]. In the mid-60s, General Motors designed the first fuel cell car, the Electrovan, which was only built as a demonstration vehicle [2]. Since then, many scientists from all over the world have been working on the “terrestrial” applications of SOFCs. However, the commercial breakthrough has still not been achieved, even though SOFCs have been marketable for quite some time [3]. One possible reason for the hampering of the commercial breakthrough is the restricted possibilities for experimental determination of the lifetime for SOFCs [4]. Indeed, the evaluation for the lifetime of SOFCs is a very time-consuming and hence expensive task, as their improvement within the last 10–15 years leads to normally very

low degradation mechanisms of only a few mV per 1000 h [5]. To overcome experimental errors and to investigate major degradation mechanisms, SOFC tests must be done over several thousand hours [6]. These tests are undertaken under galvanostatic conditions in terms of decay of cell voltage or increased cell resistance, as in particular the change in the cell resistance allows conclusions to be drawn about changes within the microstructure, the chemistry, and the stoichiometry, as well as other interactions, related to major degradation mechanisms [7]. These major degradation mechanisms include Ni-phase coarsening, Ni-phase decrease or pore structure evolution for the fuel gas electrode or Cr-poisoning, and segregation of the cathode material, as well as coarsening for the oxygen electrode [8]. Therefore, Forschungszentrum Jülich GmbH, and in particular our research group, has investigated the long-term behavior of SOFCs and their use in stacks from a couple of thousands of hours up to several years [9, 10].

This is an open access article under the terms of the [Creative Commons Attribution](https://creativecommons.org/licenses/by/4.0/) License, which permits use, distribution and reproduction in any medium, provided the original work is properly cited.

© 2025 The Author(s). *Fuel Cells* published by Wiley-VCH GmbH.

Normally, neither academia nor industry has the capacity to run cell or stack tests over such a long period of time. Therefore, other solutions must be found for the long-term performance prediction of SOCs and especially SOFCs. One solution, which would also be beneficial for later operation of these cells, would be the use of nanoparticles (NPs) to produce SOCs and SOFCs [11]. NP-based SOFCs show either an accelerated aging for long-term prediction or an analogue performance at lower temperatures of around 500°C (compared to 650–850°C of conventional SOFCs) [12]. This is mostly due to the high surface area and triple-phase boundary (TPB) length of NPs, resulting in a high electro-activity of the electrodes. Furthermore, NPs are more sinter active than conventional particles in the submicron range, resulting in a decrease of the sintering temperature during manufacturing. Hence, NP-based SOFCs can be produced and operated at lower temperatures, making them more cost-effective and more sustainable than conventional SOFCs [11]. Finally, NP-based SOFCs show high cooking/sulfur tolerance for non-H₂ fuels as well as superior thermal/chemical stability in reducing atmosphere [13]. Literature is full of more or less successful attempts to produce NP-based SOFCs. However, there are some general issues when producing those cells. In the case of Forschungszentrum Jülich GmbH, a twin-coated approach and screen printing of sol-gel-derived paste have been tested with either delamination phenomena or the formation of (micro-)cracks as outcome. Similar problems have been faced when using sol-gel methods to produce NP-based SOFCs [14, 15]. A modified sol-gel process, the Pechini method, which has been widely used to obtain nanomaterials or precursors in many fields, can be scaled up, but it is difficult to manipulate particle size, morphology, agglomeration, and sintering behavior [16]. Other more advanced technologies, such as vacuum deposition, spray pyrolysis, and metal-organic deposition, as well as spin coating, are mostly stable with a variety of modified surfaces but very limited layers with regard to their thickness [17–22]. Another important method, which has aroused more and more interest, especially within the last 10–20 years, is infiltration methods. These methods are very easy in execution and can produce NPs within a stable scaffold without the formation of cracks or delamination after heat treatment at around 500°C [11]. However, major issues in the production of such cells keep remaining, such as the reliable reproducibility of the production of the cells, the need for multiple instances of impregnation to achieve the desired loading of electrocatalysts or to form a charge carrier transfer channel/network, or the unsuitability for large-size cell fabrication due to requirement for homogeneous material distribution [23–25]. Despite these problems, infiltration experiments seemed to be an easy and good way to produce NP-based SOFCs.

Herein, we report on the use of NPs for the manufacturing of symmetrical cells. Symmetrical cells were chosen to investigate exclusively the electrochemical performance of the anode side of the cell and to exclude further possible interactions with the cathode side. Furthermore, electrolyte-supported cells were investigated for the sake of simplicity, as metal-supported cells are dense when not reduced and anode-supported cells need very high sintering temperatures for the electrolyte. Moreover, in both cases, interlayers and ideal surfaces are needed. The infiltration of the whole cell during the infiltration steps is also an issue in the case of metal-supported cells and anode-supported cells [26, 27]. Therefore, two different approaches for the manufacturing

of these cells were chosen: screen printing, which is the state-of-the-art process, and in situ synthesis of NPs through infiltration of a gadolinium-doped ceria (GDC) scaffold with an Ni(NO₃)₂ solution and vice versa. For the screen-printing method, either commercially available NP powders or lab-synthesized NPs were used and implemented into a paste [28].

2 | Experimental Procedures

2.1 | Cell Fabrication

Symmetrical cells consisting of an 8YSZ electrolyte from the company Kerafol (Eschenbach i.d.Opf., Germany) sandwiched in between a GDC interlayer were produced. The GDC powder (Gd_{0.1}Ce_{0.9}O_{1.95}) was commercially available from Fuelcellmaterials (Lewis Center, OH, USA) and transformed into a paste by the standard in-house procedure. Therefore, the GDC powder was transformed into a paste using α -terpineole as a dispersion medium and ethylcellulose as a transport medium.

For the manufacturing of the NiO:GDC functional layer, three approaches were undertaken. First, commercially available GDC nanopowders from Fuelcellmaterials and NiO nanopowders from American Elements were purchased, mixed in a 50:50 w% ratio, and once again transformed into a paste using α -terpineole as a dispersion medium and ethylcellulose as a transport medium. Second, the same procedure was done with a 50:50 w% mixture ratio of commercially available GDC nanopowders from Fuelcellmaterials and NiO submicronpowders from Vogler. Third, a paste of a 50:50 w% mixture of NiO:GDC was synthesized following a literature-known procedure. Therefore, an aqueous solution of nickel(II) nitrate, gadolinium(III) nitrate, and cerium(III) nitrate was mixed in a 50:50 vol% of Ni:GDC and added dropwise to a solution of ammonium tartrate. Upon the completion of the reaction (4 h), the precipitates were dried at 80°C overnight and calcinated at 500°C for 5 h after grounding for 15 min [28]. In both cases, the produced pastes were used for screen printing on both sides of the GDC sandwiched 8 YSZ electrolyte.

For the infiltration experiment, either an additional GDC layer or an NiO layer was screen printed on both sides of the GDC sandwiched 8 YSZ electrolyte. In the case of the additional GDC layer, an Ni(NO₃)₂ solution (3 mol) was used for the infiltration experiment. Therefore, the cells were immersed into the solution for about 5 min under vacuum, dried, and sintered at 500°C for 3 h. The infiltration of the NiO layer, on the other hand, was undertaken under the same conditions using a 3-mol solution of GDC(NO₃)₃. In both cases, different sintering temperatures for the respective scaffold were used and a variety of repetitions for the infiltration steps were tested. For the GDC scaffold, sintering temperatures of 1200°C, 1300°C, and 1400°C for 3 h each with an infiltration frequency of three, six, and nine steps were chosen. The infiltrated NiO layers, on the other hand, were sintered at 1100°C, 1200°C, and 1300°C for 3 h, beforehand. Here, again, the same number of infiltration steps were used.

In all the above-described cases, an additional contact layer of NiO was added on top using screen-printing method and dried at 80°C overnight (see Figure 1).

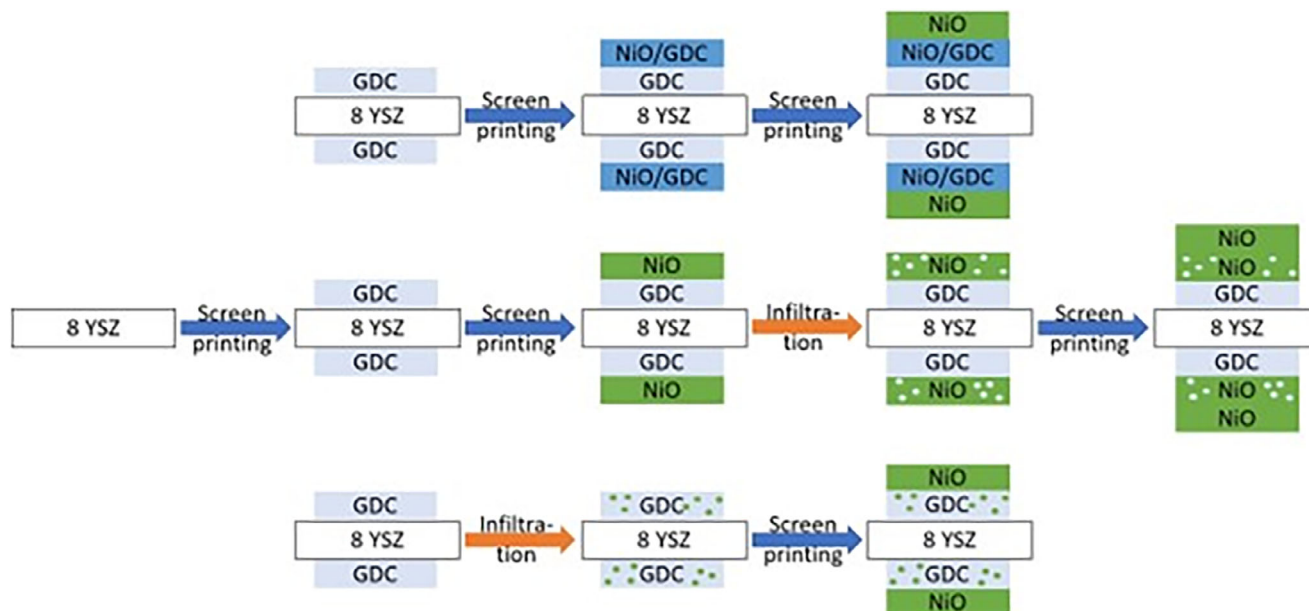


FIGURE 1 | Manufacturing scheme of symmetrical cells (infiltrated NPs are marked as green [in the case of NiO] or blue [in the case of GDC]). GDC, gadolinium-doped ceria.

2.2 | Electrochemical Characterization

For the determination of the polarization resistance (R_{pol}) of each symmetrical cell, electrochemical impedance spectroscopy (EIS) was performed. Therefore, an Alpha A high-performance frequency analyzer (Solartron 1260 Technologies; Ametek, Meerbusch, Germany) at a frequency range between 10^6 and 3×10^{-2} Hz and a response voltage of 12 mV was used. However, only the polarization resistance (R_{pol}) is of interest within this research, as the ohmic resistance (R_{ohm}), for instance, is affected by heat treatment, extra layers, and/or the device itself. Furthermore, in some of the GDC-infiltrated NiO scaffolds, a GDC coating was obtained on the top of the electrode. Therefore, Nyquist plots were obtained from the EIS measurements, whereby the ohmic resistance (R_{ohm}) was subtracted from it. For further details, see ref. [29].

2.3 | Microstructural Characterization

The specimens were sputtered with platinum to ensure sufficient electrical conductivity for investigations with a scanning electron microscope (SEM) (Zeiss CrossBeam XB 1540, Carl Zeiss AG, Oberkochen, Germany) with a mirror detector and 3 keV electron energy.

2.4 | Particle Size Characterization

The in-house particle size distribution was done by solving the GDC NPs and the NiO NPs, respectively, in ethanol. The measurement was done in three steps: first, measurement of the particle size without ultrasound; second, the measurement of the particle size with ultrasound; third, a combination of the two above-described methods.

2.5 | Stability Test

The stability of the cells was simply checked by sticking a commercially available adhesive tape onto the respective conductive layer and checking for any visible detachment after removal of the tape.

3 | Results and Discussion

3.1 | Microstructural Characterization of NiO and GDC Nanopowder

Both NiO and GDC commercial nanopowders had specifications from the manufacturer of $D_{50} < 100$ nm in the case of NiO and a specific surface area of more than $100 \text{ m}^2 \text{ g}^{-1}$ in the case of GDC. However, the in-house measured particle size distribution and the measured specific surface area of these two powders show different results (see Figure 2). The particle size distribution shows that the major fraction of the GDC powder has a particle size of about $10 \mu\text{m}$, whereas for NiO, most of the particles have a size of $5 \mu\text{m}$. The measured specific surface area, on the other hand, shows two different results. On the one hand, it confirms the aforesaid results are correct and that the received commercial powders are not within the nanosized range. On the other hand, the specific surface areas of both powders (GDC: $56.8 \text{ m}^2 \text{ g}^{-1}$ and NiO: $56.9 \text{ m}^2 \text{ g}^{-1}$) are 6–10 times higher than those of other comparable powders within the submicron range. Due to the higher specific surface areas of both powders, it can be assumed that the pristine powders were in the nano range.

To better understand this discrepancy of the two nano powders of NiO and GDC, several SEM images were taken (see Figure 3). The SEM images confirmed the measurements, indeed, and they also revealed that those particles were NPs in the pristine state. However, due to the strong agglomeration, which apparently

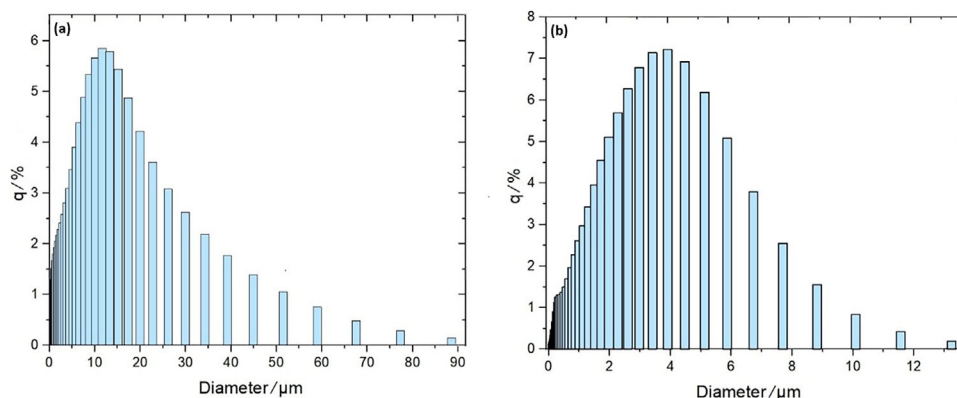


FIGURE 2 | Particle size distribution for GDC (a) and NiO (b).

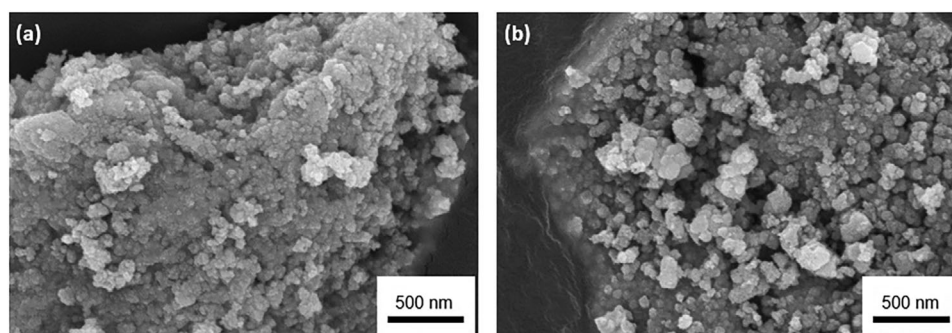


FIGURE 3 | Scanning electron microscope (SEM) (3 kV) images of GDC (a) and NiO (b).

cannot be overcome either by milling processes or even by the ultrasonification process for the preparation for the measurement of the particle size distribution, these commercially available powders cannot be considered “real” NPs. Yet, they were used for the transformation into a paste, as the measured specific surface area is closer to the size range of NPs than other comparable powders within the submicron range.

3.2 | Changes of the Parameters for the Paste

A variety of parameters to produce an NP-based paste were investigated to improve the stabilization of the resulting symmetrical cells. First, different suspension media, such as polyvinylpyrrolidone in water or polyvinylalcohol in ethanol in different compositions (2, 5, and 10 w%) as well as α -terpineole were tested to have an ideal solid distribution and to investigate the drying behavior. Second, different transport agent suspensions, such as 6 w% ethylcellulose in α -terpineole with a chain length of 10 cp, 6 w% ethylcellulose in α -terpineole with a chain length of 45 cp, or 15 w% ethylcellulose in α -terpineole with a chain length of 45 cp, were used. In that, the influence of the transport agent regarding viscosity as well as green density could be investigated. Furthermore, the chain length could have had an influence on the distribution of the solid particles within the paste. Although all these preliminary tests resulted in an acceptable paste, the stability of the symmetrical layers could not be improved. Finally, the solid loading of the paste was changed in a range between 20 w% and a maximum of 60 w%, which was also investigated

for an ideal sintering behavior through a maximum of the solid loading of the paste and its stability with respect to the later cells. In all cases, no positive intermediate results could be achieved.

3.3 | Insufficient Adhesion of the Screen-Printed Symmetrical Cells

All the pastes described in Section 3.2 lead to a variety of different outcomes, with the same result. Neither the mixture of the commercially available NiO and GDC nanopowders nor the synthesized NPs from the literature's known procedure led to stable symmetrical cells. Although the NiO/GDC conductive layer of the symmetrical cells with the mixture of the commercially available NiO and GDC nanopowders flaked off after sintering in a range between 1100°C and 1400°C for 3 h, the NiO/GDC conductive layer of the symmetrical cells with the synthesized NP from the literature-known procedure was stable enough to undertake EIS measurements and to characterize their electrochemical behavior. Indeed, even at a higher sintering temperature of 1400°C, the NiO/GDC conductive layer of the symmetrical cells with the mixture of the commercially available NiO and GDC nanopowders not only flaked off but also showed this behavior over a greater area compared to the ones at lower sintering temperatures (see Figure 4).

In the case of the NiO/GDC conductive layer of symmetrical cells with the synthesized NP from the literature's known procedure, on the other hand, the increase of the sintering temperature

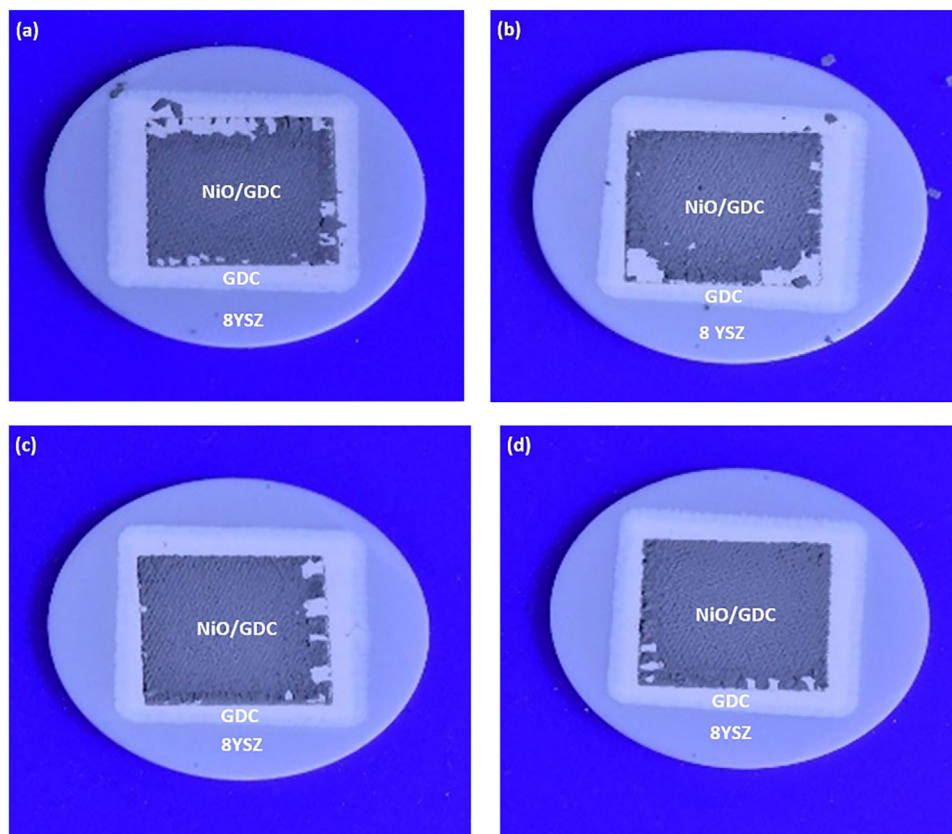


FIGURE 4 | Optical pictures of symmetrical cells at different sintering temperatures for 3 h. Sintering temperature: 1400°C (a); sintering temperature: 1300°C (b); sintering temperature: 1200°C (c); and sintering temperature: 1100°C (d).

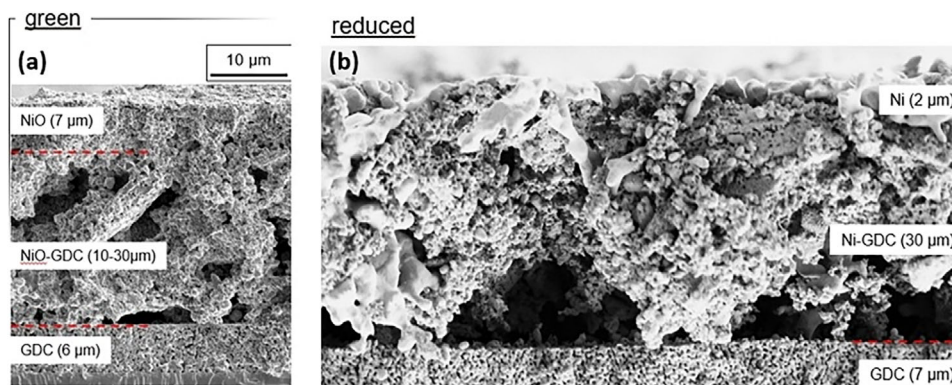


FIGURE 5 | Scanning electron microscope (SEM) (3 kV) images of symmetrical cells with NP from literature known procedure (sintering temperature = 1400°C) in the green state (a) and after reduction (b).

leads, as expected, to a densification of the conductive layer. However, here, again, a higher sintering temperature did improve the stabilization of the symmetrical cells only slightly, and delamination still occurred. Even an increased sintering time at a sintering temperature as high as 1400°C did not show any major beneficial increase in the stability of the conductive layer (see Figure 5).

These observations can be explained by several reasons: First, the produced cells have a relatively small area of only 1 cm² compared to a great circumference of 4 cm, which leads to a greater influence of edge effects in comparison to larger cells.

Second, during the sintering process, two phenomena happen simultaneously in the green layer, competing with each other and consequently destabilizing the whole symmetrical cells. The particles within the green layer sinter together, which makes the layer denser. The particles on the interface between the green layer and the 8YSZ substrate, on the other hand, sinter together at the same time. These two reactions create tensions within the green layer, leading probably to cracks, which is even more supported by the large surface of the NPs (see Figure 6).

To avoid the above-mentioned issues, another approach was tested. The mixture of NiO-submicron powder and GDC-

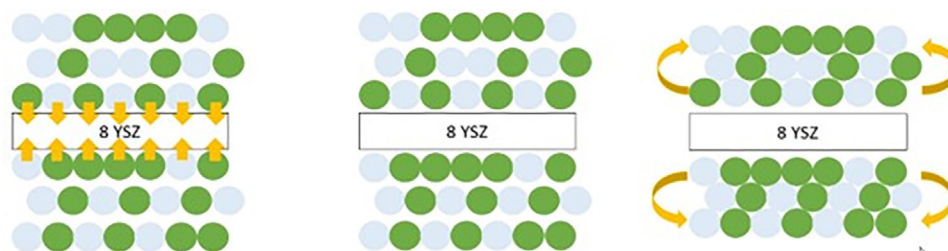


FIGURE 6 | Shrinkage behavior of NiO and GDC particles during sintering. Sintering behavior of NPs on the interface between conductive layer and 8YSZ electrolyte (left), and between the NPs (right).

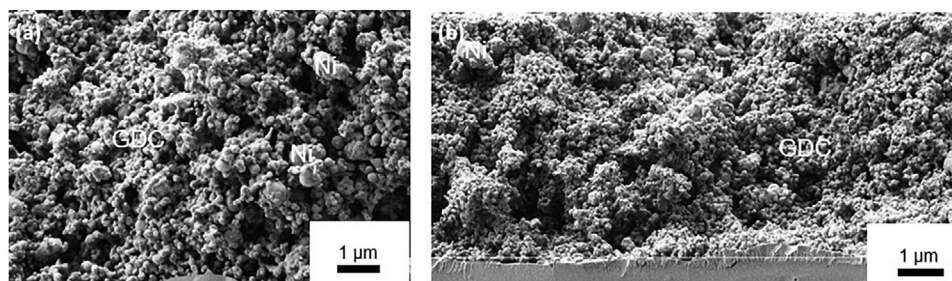


FIGURE 7 | Scanning electron microscope (SEM) (3 kV) images of symmetrical cells with GDC-NP from Fuelcellmaterials and NiO-submicron powders from Vogler (sintering temperature = 1080°C) in different magnifications. (a) The SEM image shows the better adhesion of the NiO/GDC conductive layer; (b) the SEM image is a larger overview. GDC: gadolinium-doped ceria.

nanopowder was used to create stable cells by giving the smaller NPs enough connecting points with the bigger submicron powders to remove internal tension within the conductive layer. This approach was marked by greater success, and even after reduction, the conductive layer showed neither exfoliation nor delamination (see Figure 7).

3.4 | NiO-Infiltrated GDC Scaffolds and GDC-Infiltrated NiO Scaffolds

After various attempts of different binders, transport media, solid loads, and sintering temperatures as well as sintering times, a different solution was used for the manufacturing of symmetrical NP-based cells: Infiltration. Therefore, two ways were investigated: the infiltration of a GDC scaffold with NiO NPs and the infiltration of an NiO scaffold with GDC NPs. In both cases, the respective conductive layer of the symmetrical cells was stable, and neither delamination nor flaking occurred after sintering or EIS measurements. Both cell types were investigated via SEM, and the resulting images are depicted in Figure 8. Indeed, not only are these two cell types stable enough to prevent delamination, but they also include the desired NPs with a size down to 10 nm. With this result, the symmetrical cells were used for EIS measurements and for characterization of their electrochemical behavior.

3.5 | Electrochemical Characterization

The electrochemical characterization of the different symmetrical cells shows two interesting results: First, a minimum of the polarization resistance was achieved with a sintering temperature

of 1100°C and a repetition of the infiltration steps of nine times for the NiO scaffold. This is of particular interest, as a higher number of infiltration steps are suspected to lead to greater conductivity due to the higher concentration of GDC within the NiO scaffold. However, it seems that too many repetitions of the infiltration steps lead to a blockage of the pores within the NiO scaffold and therefore to a reactant depletion at the TPBs and GDC surfaces. Even the sintering temperature of 1100°C seems to be optimal with a good compromise between reduced adhesion and strong densification. Second, the use of NP-based symmetrical cells does indeed improve their electrochemical performance compared to those using particles with the submicron range (see Figure 9: Only the EIS measurement for the best performed infiltrated samples are shown). This is even the case when the lab-synthesized NPs were used and the conductive layer delaminated after EIS measurements. Moreover, the herein reported symmetrical cells with an NiO scaffold show an improved electrochemical performance compared to literature-known values. In general, however, the symmetrical cells with a GDC scaffold and NiO NPs indicate excellent performance, which is in good agreement with the literature [30].

4 | Discussion

The present investigations have shown a variety of different results. The adhesive problems with pure NPs for screen-printing method can be solved by mixing NPs with particles in the submicron range. However, the electrochemical performance is not as good as the electrochemical performance achieved by anodes using particles purely in the submicron range. This can be explained by the fact that there are probably still some adhesive problems between the NPs and the particles in the

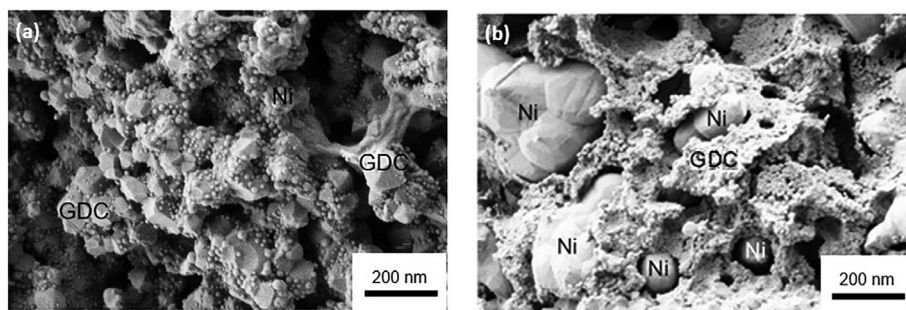


FIGURE 8 | Scanning electron microscope (SEM) (3 kV) images of GDC-infiltrated NiO scaffold (a) and NiO-infiltrated GDC scaffold (b). GDC, gadolinium-doped ceria.

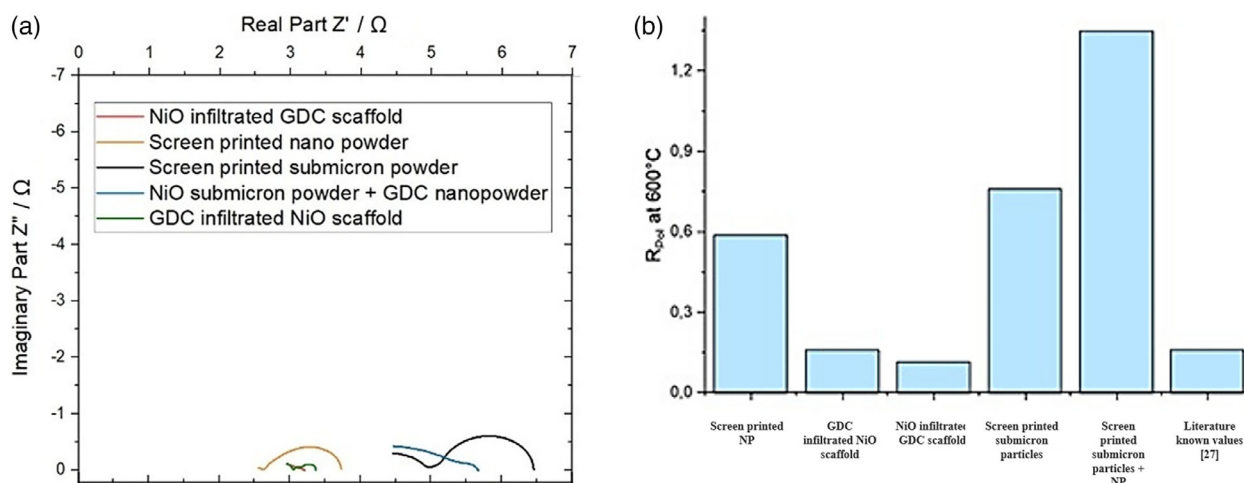


FIGURE 9 | EIS measurement for symmetrical cells (a) and comparison of the R_{pol} (b). GDC, gadolinium-doped ceria; NP, nanoparticle.

submicron range within the conductive layer. This leads to a reduced concentration of TPBs. Surprisingly, the electrochemical performance of the anode using NPs from the literature-known process is improved compared to that of the anodes using particles in the submicron range. Here, the adhesion between the conductive layer and the electrolyte is probably strong enough for the EIS measurement. However, the pores that emerge from the reduction step during this measurement destabilize the conductive layer to a sufficient extent. The ideal stability as well as the best electrochemical performance was achieved with the infiltration experiments. The produced anodes did not show any signs of delamination, and the electrochemical performances are in good agreement with literature-known values. Indeed, the infiltration of GDC NPs into the NiO scaffold is even better than those found in literature. Hereby, a higher content of TPB and, therefore, geometrically enhanced electrode performance can be found, which can be explained by a high density of GDC NPs. This is in good agreement with the literature [31, 32]. The infiltration of NiO NPs, on the other hand, cannot reach the same R_{pol} values as those found in the literature. This can be explained by the different manufacturing methods, such as higher sintering temperature of the conductive layers or infiltration steps. Former can lead to an increased density of the conductive layer and consequently a decreased gas diffusion. The latter can cause an insufficient electron transport, as the electronic conductivity of GDC is several orders of magnitude lower than Ni, for example, only $4.7 \times 10^{-1} \text{ S cm}^{-1}$ at 700°C [32, 33].

5 | Conclusion

In conclusion, two different ways were investigated for the manufacturing of symmetrical NP-based cells: screen printing and infiltration. Although it was not possible to produce stable cells via screen printing only using NPs, due to a lack of adhesive force between the NPs themselves within the conductive layer as well as between the NPs and the GDC interlayer, the mixture of NPs and submicron particles showed some promising results. The infiltration of the GDC scaffold as well as the NiO scaffold was also successful. Indeed, both the infiltration of GDC NPs within an NiO scaffold and the infiltration of NiO NPs with a GDC scaffold produced stable symmetrical NP-based cells with particle size down to 10 nm. Both cell types were investigated regarding their electrochemical behavior, and both showed a three to four times improved performance compared to symmetrical cells using particle sizes within the submicron range. Furthermore, these electrode types can now be used to produce SOFCs. These SOFCs are objectives for the investigation of long-term behavior and to investigate major degradation mechanisms.

Acknowledgments

The project “WirLebenSOFC” was funded by the German Federal Ministry for Economic Affairs and Climate Protection (BMWK), which is gratefully acknowledged (Contract No. 03SF0622B). We thank Dr.

Sebold Doris for the SEM images of the GDC and NiO NPs, Dr. Florian Wankmüller for the SEM images of the symmetrical cells, and Andrea Hilgers for the particle size distribution.

Open access funding enabled and organized by Projekt DEAL.

Conflicts of Interest

The authors declare no conflicts of interest.

Data Availability Statement

The data that support the findings of this study are available from the corresponding author upon reasonable request.

References

1. R. W. Groove, "Volta'sche Säule von grosser elektro-chemischer Kraft," *Annals of Physics* 124, no. 10 (1839): 300.
2. A. Adler, 50-year-old Electrovan was first fuel cell technology transfer from JFK's moonshot challenge, <https://phys.org/news/2016-10-year-old-electrovan-fuel-cell-technology.html>.
3. N. H. Behling, *Fuel Cells—Current Technology Challenges and Future Research Needs* (Elsevier, 2013).
4. S. Z. Golkhatmi, M. I. Asghar, and P. D. Lund, "A Review on Solid Oxide Fuel Cell Durability: Latest Progress, Mechanisms, and Study Tools," *Renewable & Sustainable Energy Reviews* 161 (2022): 112339.
5. S. C. Singhal, *Solid Oxide Fuel Cells: Facts and Figures*, ed. J. T. S. Irvine (Springer, 2013).
6. A. Ploner and A. Hagen, "Study of Operating Parameters for Accelerated Anode Degradation in SOFCs," *Fuel Cells* 17 (2017): 498–507.
7. R. S. Gemmen, M. C. Williams, and K. Gerdes, "Degradation Measurement and Analysis for Cells and Stacks," *Journal of Power Sources* 184 (2008): 251–259.
8. M. V. Ananyev, D. I. Bronin, D. A. Asinkin, et al., "Characterization of Ni-Cermet Degradation Phenomena I. Long Term Resistivity Monitoring, Image Processing and X-Ray Fluorescence Analysis," *Journal of Power Sources* 286 (2015): 414–426.
9. I. D. Unachukwu, V. Vibhu, I. C. Vinke, R.-A. Eichel, and L. G. J. de Haart, "Electrochemical and Degradation Behaviour of Single Cells Comprising Ni-GDC Fuel Electrode Under High Temperature Steam- and Co-Electrolysis Conditions," *Journal of Power Sources* 556 (2023): 232436.
10. N. H. Menzler, D. Sebold, Y. J. Sohn, and S. Zischke, "Post-Test Characterization of a Solid Oxide Fuel Cell After More Than 10 Years of Stack Testing," *Journal of Power Sources* 478 (2020): 228770.
11. L. Fan, B. Zhu, P.-C. Su, and C. He, "Nanomaterials and Technologies for Low Temperature Solid Oxide Fuel Cells: Recent Advances, Challenges and Opportunities," *Nano Energy* 45 (2018): 148–176.
12. Y. Liu, Z. Shao, T. Mori, and S. P. Jiang, "Development of Nickel Based Cermet Anode Materials in Solid Oxide Fuel Cells—Now and Future," *Materials Reports: Energy* 1 (2021): 100003.
13. Z. Xie, M. Zhang, Y. Yi C, et al., "Nanostructured Fuel Electrodes for Low-Temperature Proton- and Oxygen-Ion-Conducting Solid Oxide Cells," *Journal of Energy Chemistry* 106 (2025): 302–330.
14. R. Hansch, D. Lavergnat, N. H. Menzler, and D. Stöver, "Nanocrystallized Ytria-Stabilized Zirconia for Solid Oxide Fuel Cell Applications," *Advanced Engineering Materials* 7 (2005): 142–144.
15. R. Hansch, M. R. R. Chowdhury, and N. H. Menzler, "Screen Printing of Sol-Gel-Derived Electrolytes for Solid Oxide Fuel Cell (SOFC) Application," *Ceramics International* 35 (2009): 803–811.
16. J. Serra, S. Uhlenbruck, W. Meulenberg, H. Buchkremer, and D. Stöve, "Nano-Structuring of Solid Oxide Fuel Cells Cathodes," *Topics in Catalysis* 40 (2006): 123–131.
17. J. Januschewsky, M. Ahrens, A. Opitz, F. Kubel, and J. Fleig, "Optimized $\text{La}_{0.6}\text{Sr}_{0.4}\text{CoO}_{3-\delta}$ Thin-Film Electrodes With Extremely Fast Oxygen-Reduction Kinetics," *Advanced Functional Materials* 19 (2009): 3151–3156.
18. G. J. la O, S. J. Ahn, E. Crumlin, et al., "Catalytic Activity Enhancement for Oxygen Reduction on Epitaxial Perovskite Thin Films for Solid-Oxide Fuel Cells," *Angewandte Chemie International Edition* 49 (2010): 5344–5347.
19. S. Wang, J. Yoon, G. Kim, D. Huang, H. Wang, and A. J. Jacobson, "Electrochemical Properties of Nanocrystalline $\text{La}_{0.5}\text{Sr}_{0.5}\text{CoO}_{3-x}$ Thin Films," *Chemistry of Materials* 22 (2010): 776–782.
20. R. Sayers, N. L. O. Flack, J. Alaria, et al., "Epitaxial Growth and Enhanced Conductivity of an IT-SOFC Cathode Based on a Complex Perovskite Superstructure With Six Distinct Cation Sites," *Chemical Science* 4 (2013): 2403–2412.
21. A. M. Saranya, D. Pla, A. Morata, et al., "Engineering Mixed Ionic Electronic Conduction in $\text{La}_{0.8}\text{Sr}_{0.2}\text{MnO}_{3+\delta}$ Nanostructures Through Fast Grain Boundary Oxygen Diffusivity," *Advanced Energy Materials* 5 (2015): 1500377.
22. J. Pan, Y. Ye, M. Zhou, et al., "Improving the Activity and Stability of Ni-Based Electrodes for Solid Oxide Cells Through Surface Engineering: Recent Progress and Future Perspectives," *Materials Reports: Energy* 1 (2021): 100025.
23. T. Sholklipper, C. Lu, C. Jacobson, S. Visco, and L. De Jonghe, "LSM-Infiltrated Solid Oxide Fuel Cell Cathodes," *Electrochemical and Solid-State Letters* 9 (2006): A376.
24. K. J. Yoon, M. Biswas, H.-J. Kim, et al., "Nano-Tailoring of Infiltrated Catalysts For High-Temperature Solid Oxide Regenerative Fuel Cells," *Nano Energy* 36 (2017): 9.
25. J. Chen, F. Liag, D. Yan, et al., "Performance of Large-Scale Anode-Supported Solid Oxide Fuel Cells With Impregnated $\text{La}_{0.6}\text{Sr}_{0.4}\text{Co}_{0.2}\text{Fe}_{0.8}\text{O}_{3-\delta}+\text{Y}_2\text{O}_3$ Stabilized ZrO_2 Composite Cathodes," *Journal of Power Sources* 195 (2010): 5201–5205.
26. Z. Zhou, V. K. Nadimpalli, D. B. Pedersen, and V. Esposito, "Degradation Mechanisms of Metal-Supported Solid Oxide Cells and Countermeasures: A Review," *Materials* 14 (2021): 3139.
27. C. Mallon and K. Kendal, "Sensitivity of Nickel Cermet Anodes to Reduction Conditions," *Journal of Power Sources* 145 (2005): 154–160.
28. M. Choolaei, Q. Cai, and B. H. Horri, "Green Synthesis and Characterisation of Nanocrystalline NiO-GDC Powders With Low Activation Energy for Solid Oxide Fuel Cells," *Ceramics International* 47 (2021): 32804–32816.
29. Y. Liu, F. Wankmüller, T. P. Lehnert, M. Juckel, N. H. Menzler, and A. Weber, "Comparing the 3D Morphology of Solid-Oxide Fuel Cell Anodes for Different Manufacturing Processes, Annealing Times, and Operating Temperatures," *Fuel Cells* 23 (2023): 430.
30. M. Lomberg, E. Ruiz-Trejo, G. Offer, and N. P. Brandon, "Characterization of Ni-Infiltrated GDC Electrodes for Solid Oxide Cell Applications," *Journal of The Electrochemical Society* 161 (2014): F899–F905.
31. S. P. Jiang, S. Zhang, Y. D. Zhen, and W. Wang, "Fabrication and Performance of Impregnated Ni Anodes of Solid Oxide Fuel Cells," *Journal of the American Ceramic Society* 88 (2005): 1779–1785.
32. B. Mitchell-Williams, R. I. Tomov, S. A. Saadabadi, et al., "Infiltration of Commercially Available, Anode Supported SOFC's Via Inkjet Printing," *Materials for Renewable and Sustainable Energy* 6 (2017): 12.
33. L. Guesnet, G. Aubert, S. Hubert, P. M. Geffroy, C. Aymonier, and J. M. Bassat, "Infiltration of Nickel and Copper Catalysts Into a GDC Backbone Assisted by Supercritical CO_2 for Efficient SOFC Anodes," *Sustainable Energy Fuels* 6 (2022): 1801–1811.